Estudio de Robustez vs Vibración en el Control por Modos Deslizantes
Robustness vs Chattering-effect study for the Sliding Mode Control

Sergio Álvarez Rodríguez[1]

[1] Instituto Tecnológico José Mario Molina Pasquel y Henríquez. Jalisco, México

Autor para correspondencia: Sergio Álvarez Rodríguez, E-mail: ser@cio.mx; sergio.alvarez@lagos.tecmm.edu.mx

Resumen

En la literatura de control por Modos Deslizantes, un popular paradigma dice que el llamado "efecto de vibración" (vibraciones mecánicas indeseables en la planta a controlar) puede ser reducido o inclusive eliminado sin afectar la robustez del control. No obstante, los resultados de implementaciones prácticas, apoyan la idea de que esto no es necesariamente cierto. En este trabajo, se presenta un estudio del desempeño real de los Modos Deslizantes de alto orden usados como la ley de control para un sistema con múltiples entradas múltiples salidas, a partir del cual se ofrecen hallazgos interesantes del comportamiento real de la robustez del sistema de control cuando el efecto de vibración cambia en magnitud. En este estudio, para lograr la reducción de la cantidad de vibración, se utiliza el algoritmo de control llamado Super-Twisting, y la planta a controlar es un brazo manipulador de 3-GdL. Los resultados de este trabajo muestran que cuando se usan técnicas para reducir el efecto de vibración, se debe tomar en cuenta que la robustez del sistema de control también se verá afectada, y que los logros aclamados por la teoría, deben ser acotados cuando se realizan las correspondientes implementaciones prácticas.

Palabras clave: algoritmo Super-Twisting; efecto de vibración; robustez del sistema; robot manipulador de 3-GdL

Abstract

In Sliding Modes control literature, a popular paradigm says that the so called "chattering-effect" (undesirable mechanical vibrations on the plant under control) can be reduced or even removed at all without affecting the control robustness. Nevertheless, results of practical implementations support that this is not necessarily true. In this work, the actual behaviour of a class of high order Sliding Modes used as the control law for a Multiple-Input Multiple-Output system is presented, where the real performance of system robustness is studied when the chattering-effect change in magnitude. In this study, to achieve the chattering reduction, the Super-Twisting algorithm is used, and the plant to control is a 3-DoF robot arm. The results of this work show that when techniques to reduce the chattering-effect are utilized, the corresponding reduction in system robustness should also be taken into account, and that achievements of theoretical concepts must be bounded when they are implemented in practical applications.

Keywords: Super-Twisting algorithm; chattering-effect; system robustness; 3-DoF robot arm

Introduction

In (Utkin *et al*., 1999), it is set that: "systems with Sliding Modes (SM) have proven to be an efficient tool to control complex high order nonlinear dynamic plants operating under uncertainty conditions". In fact, SM dynamics may appear in systems governed by ordinary differential equations with discontinuous terms (Furuta & Pan, 2000), and it may happen that a control which depends on a function of the system state switches at high (theoretically infinite) frequency, this motion is called *sliding mode*.

In Sliding Modes Control (SMC) literature, there exist a wide range of research information about Conventional SM (CSM) (Loukianov *et al*., 2002), and Second Order SM (SOSM) (Sira-Ramírez, 2002), which are a modality of High Order SM (HOSM) (Furuta & Pan,

2003). The order of the differential equation which is the dynamical model for the SM, defines the order of the SM system. CSM are defined as first order SM, and examples for HOSM are: Twisting, Super-Twisting, Integral, Drift, and Sub-optimal SM algorithms, among others.

L. Fridman in (Fridman *et al.*, 2011) says that: By the early 80's, the control community had understood that the main disadvantage of SMC is the chattering-effect (Bartolini, 1989; Bartolini, 2002; Boiko & Fridman, 2005; Dorel & Levant, 2008; Fridman, 2001). It has been shown that this effect is mainly caused by unmodelled cascade dynamics which increase the system's relative degree (Levant, 2013) and perturb the ideal SM existing in the system. In practice, the chattering-effect is caused by the switching of the control signal, provoking high frequency mechanical vibrations, heat, mechanical wear, noise, and other drawbacks in the plant under control. In order to overcome the chattering problem in the SM, the SOSM concept was introduced in the Ph.D. dissertation of A. Levant.

It is widely accepted that the Super-Twisting Algorithm (STA) produces low operational frequencies and smooth control signals for the systems to be controlled, removing the chattering-effect without loss of robustness. This fact is claimed in SMC literature by many ways (*e.g.*, by mathematical, simulation, and/or real-time approaches), nevertheless, these studies can be bounded by some considerations.

Motivation. Even when theory says that HOSM reject the chattering without lost of robustness, the author of this work has found via practical implementations, that when the chattering is reduced, also the control robustness decreases. As there is a large gap between theory and practice, the author was motivated to carry out a study at this respect.

A small remark about this theme is made by (Alvarez, Castañeda, Jurado, Morfín, & Esquivel, 2015).

Contribution. The main contribution of this work is to show, via simulation results, that the robustness of the closed-loop control system is proportional to the amount of chattering-effect affecting the plant under control, when the HOSM technique is used.

This leads to new approaches related to this subject, since results of this nature have not been presented yet in control literature. These results will help to clarify the optimal way in which HOSM should be used in industrial applications.

The remainder of the document is organized as follows: in section 2, the closed-loop control system as the platform to obtain simulation results is presented; section 3 is devoted to

show simulation results for the robust performance when the chattering is affected; in section 4, the discussion is presented for the analysis of results; finally, concluding remarks are presented in section 5.

Closed-loop control system

This section is devoted to present the control scheme used to obtain the system robust performance when the value of the chattering-effect is moved. The closed-loop control system used to obtain reliable simulation results is a Multiple-Input Multiple-Output (MIMO) system, which includes:

1. A serial three Degrees of Freedom (3-DoF) robot arm, which is the plant to be controlled.
2. A High Order Sliding Modes (HOSM) controller, which forces the movement of the system variables toward the sliding manifold. For the case under study, the STA is employed.
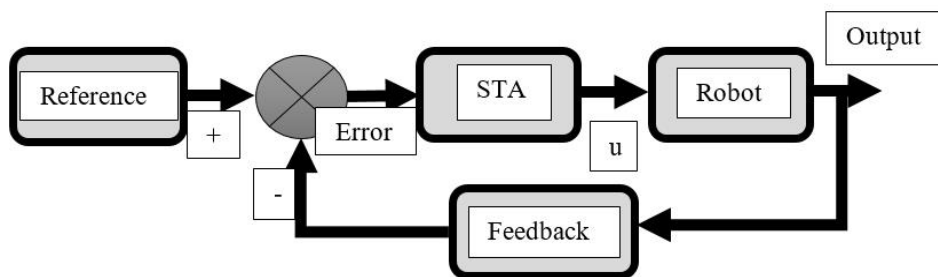
Fig. 1. Block diagram for the closed-loop control system.

Fig. 1 shows that both the reference signal and the feedback (actual position of the robot), arrive to the subtraction node to obtain the tracking error. The STA utilizes this error to generate the control signal **u** for the robot.

A serial robotic plant was selected, because it's highly coupled dynamics increase the chattering-effect from the *i*-th to the *(i+1)*-th joint. The STA was selected, because it presents the smoothest control signal among the HOSM.

The 3-DoF robot arm as the plant to be controlled

The MIMO mechanical configuration of the robot considered for this work is a 3-DoF Selective Compliant Articulated Robot for Assembly (SCARA) (Spong & Vidyasagar, 1989), also see (Qu & Dawson, 1995), which is given in a numerical state space representation by:

$$\dot{\chi}_1 = \chi_2$$
$$\dot{\chi}_2 = -M^{-1}\left[C\chi_2 + F_g + F_f\right] + M^{-1}u$$
$$y = \begin{bmatrix} \chi_1 & \chi_2 \end{bmatrix}^T + \delta(t)$$

$$M(\chi_1) = \begin{bmatrix} 1.23 + 0.1\cos(q_2) & 0.64 + 0.051\cos(q_2) & 0 \\ 0.64 + 0.051\cos(q_2) & 0.64 & 0 \\ 0 & 0 & 0.5 \end{bmatrix}$$

$$C(\chi_1, \chi_2) = \begin{bmatrix} -0.102\sin(q_2)q_2 & -0.051\sin(q_2)q_2 & 0 \\ 0.051\sin(q_2)q_1 & 0 & 0 \\ 0 & 0 & 0 \end{bmatrix}$$

$$F_g^T(\chi_1) = \begin{bmatrix} 0 & 0 & -4.905 \end{bmatrix}^T$$

$$F_f^T(\chi_1, \chi_2) = \begin{bmatrix} 1.86q_1 + 1.93\,si\,gn(q_1) \\ 0.16q_2 + 0.3sign(q_2) \\ 0.1q_3 + 0.2sign(q_3) \end{bmatrix}$$

$$\tag{1}$$

Where $\chi_1 = \begin{bmatrix} q_1 & q_2 & q_3 \end{bmatrix}^T$ and $\chi_2 = \begin{bmatrix} \dot{q}_1 & \dot{q}_2 & \dot{q}_3 \end{bmatrix}^T$ are the articular position and articular velocity respectively; y is the actual system output; $M = M(\chi_1) \in R^{3\times3}$ is the inertia matrix; $C = C(\chi_1, \chi_2) \in R^{3\times3}$ represents the Coriolis and centripetal enforces; $F_g = F_g(\chi_1) \in R^3$ is the gravitational torque vector acting over the robot arm; $F_f = F_f(\chi_1, \chi_2) \in R^3$ is the torque vector due to friction forces; $u \in R^3$ represents the system control signal; and $\delta(t) \in R^6$ is a function which represents non-modelled dynamics, parametric variations, system noise and external perturbations. In a closed-loop control system, χ_1 and χ_2 become contaminated with $\delta(t)$. It is important to set that the dimension of the state space -represented by n- has the value of 2 (*i.e.*, $n = 2$). Equation (1) represents an actual robot arm (to see details about this robot see (Álvarez & Castañeda, 2015)).

Super-Twisting algorithm

Theoretical details of the STA are presented in (Fridman, Moreno, & Iriarte, 2011; Levant, 1993) among others. Taking the STA for the MIMO system as:

$$u(t) = u_1(t) + u_2(t)$$
$$u_1(t) = -\alpha \mid \chi_1(t) \mid^{\frac{1}{2}} \operatorname{sgn}\left[\chi_1(t)\right]$$
$$\dot{u}_2(t) = -\beta \operatorname{sgn}\left[\chi_1(t)\right]$$

$$(2)$$

Where $u(t) \in R^3$ is the closed-loop control signal which forces the movement of the system variables toward the sliding manifold; $\alpha \in R^3$ and $\beta \in R^3$ are the Super-Twisting *positive* adaptive parameters.

Moreover, for some positive constants Φ, Γ_m, and Γ_M, the corresponding sufficient conditions for the finite time convergence of the STA to the sliding manifold are:

$$\beta > \frac{\Phi}{\Gamma_m}$$

$$\alpha^2 \geq \frac{\Gamma_M(\beta+\Phi)}{\Gamma_m^3(\beta-\Phi)}$$

(3)

As the state space representation in (1) can take the form:

$$\dot{\chi}_1 = \chi_2$$
$$\dot{\chi}_2 = f(\chi_1,\chi_2) + g(\chi_1,\chi_2)u$$

From which the following conditions are needed (see (Levant, 1993; Morfín, 2009)):

$$\Phi \geq \|\dot{f}(\chi_1,\chi_2)\| + U_0\|\dot{g}(\chi_1,\chi_2)\|$$
$$0 \leq \Gamma_m \leq \|g(\chi_1,\chi_2)\| \leq \Gamma_M$$

(4)

Where U_0 represents the operational limits of the plant to control.

Simulation results

To implement the control system the following general conditions and parameters for the control model are taken:

1. Initial conditions for the robot at 1.5 *rad*.
2. Computing sampling time is 0.005 s.

The reference signals to track for the first, second and third robot joints are shown in Table 1, where it can be seen that sine wave forms were selected with their own amplitudes and frequencies which are different from each other. The purpose to select these parameters in this way is to cause disturbance effects between joints, which simulates a behaviour more attached to reality.

Table 1. Reference signals to track.

Joint (DoF)	Function (f(x)=)	Amplitude [rad]	Frequency [Hz]	Phase [rad]
1	sine wave	1	1	0
2	sine wave	3	2	0
3	sine wave	5	3	0

It is important to note that for simulations made in this work, initial conditions for the robot are out from the reference signals (*i.e.*, the robot joints start at 1.5 *rad*, while the reference signals have a *phase* = 0), this can be considered as a disturbance by nature. Finally, gravity is an important kind of disturbance to account in robotics.

In the beginning of experiments made under the specified conditions, heuristically it was found that there exist an unstable region for the STA working under certain values for the α and β gains of the STA. This unstable region corresponds to the second range of values given by Table 2. Thus, there are two available operational ranges to work (*i.e.*, the "1*st* range: low" and the "3*rd* range: high"). Evidently, the upper limit of the 1*st* range, corresponds to the lower limit of the 2*nd* range, and the upper limit of the 2*nd* range, corresponds to the lower limit of the 3*rd* range.

Table 2. Values for the three ranges of the STA gains.

Joint No. (DoF)	Range values for α	Range values for β
1st range: low		
1	$\approx 0.1 - 95$	$\approx 0.1 - 550$
2	$\approx 0.1 - 95$	$\approx 0.1 - 570$
3	$\approx 0.1 - 100$	$\approx 0.1 - 600$
2nd range: unstable		
1	$95 - 6.8 \times 10^6$	$550 - 55 \times 10^6$
2	$95 - 7.4 \times 10^6$	$570 - 57 \times 10^6$
3	$100 - 7.2 \times 10^6$	$600 - 60 \times 10^6$
3rd range: high		
1	$6.8 \times 10^6 - \inf$	$55 \times 10^6 - \inf$
2	$7.4 \times 10^6 - \inf$	$57 \times 10^6 - \inf$
3	$7.2 \times 10^6 - \inf$	$60 \times 10^6 - \inf$

Moreover, it is easy to see that there is a wide range of values for Φ, Γ_m, and Γ_M to satisfy conditions (3)–(4) with the α, β values of both the 1*st* and the 3*rd* ranges in Table 2, which accomplishes:

$$kx\left(t_0\right) k < \gamma \Rightarrow kx\left(t\right) k \leq b, \forall t \geq t_0 + T$$

(5)

Where there exist positive constants b and c, for every $\gamma \in (0,c)$, a positive constant $T = T(\gamma)$, and with arbitrarily large value for γ, then the solutions for the system working under conditions of 1*st* and 3*rd* ranges are said to be *globally uniformly ultimately bounded* (see (Khalil, 2001)). Then, Table 2 is the first result obtained in this work and sets the basis for the results given by Figs. 2–16.
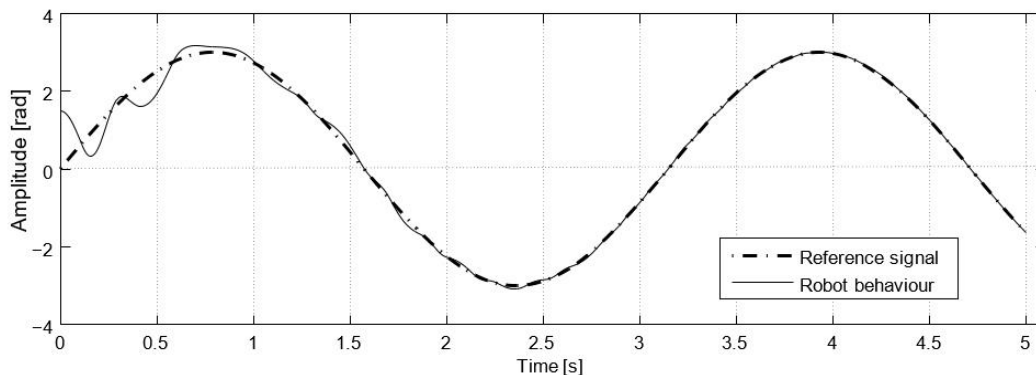
Figs. 2–4 are devoted to show the trajectory tracking for the first, second and third robot joints respectively, working with the upper limits of the α, β values located in the 1*st* range.

In Fig. 2 it can be seen that inside 2.5 s there are still effects of the transient stage, and a pseudo convergence is reached after 3 s. Also it can be seen that, as a result of the disturbance provoked by the movement of second link, the first joint comes out completely from its reference signal in the region between 4 and 4.8 s.
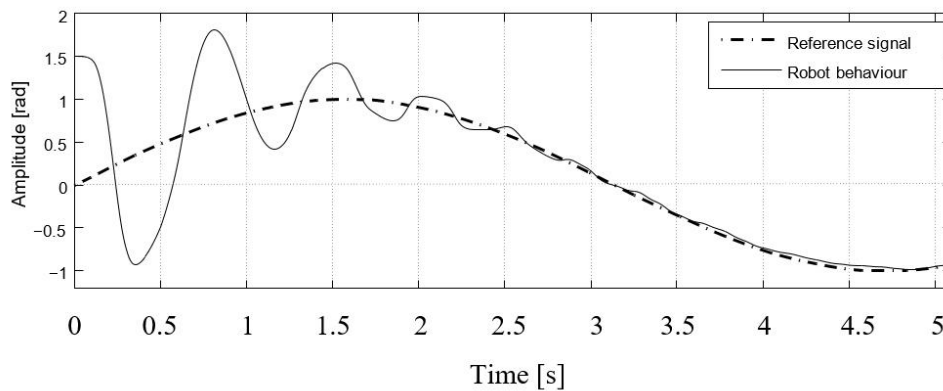
Fig. 2. Robot's first joint tracking the reference with $\alpha = 95$ and $\beta = 550$.

Fig. 3 shows that inside 1.25 *s* there are still effects of the transient stage. In steady state, a better convergence than that obtained by the first joint is reached, but still, the interference caused by the first joint is visible.

**Fig. 3.** Robot's second joint tracking the reference with $\alpha = 95$ and $\beta = 570$.

Fig. 4 shows the beginning of a pseudo convergence after 4.2 *s*. The transitional stage is quite extensive compared with the two previous. Nearby the time values 1.5, 2.6 and 3.6 *s*, it can be seen clearly the effect of gravity, acting as a disturbance force.
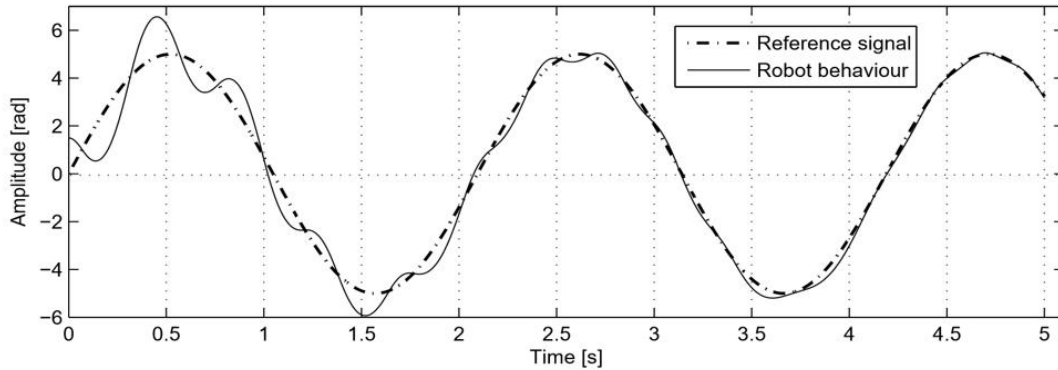

Fig. 4. Robot's third joint tracking the reference with $\alpha = 100$ and $\beta = 600$.

Figs. 5–7 are dedicated to show the control signal provided by the controller for the first, second and third robot joints respectively, working with the upper limits of the α, β values located in the 1*st* range.

The control signal appearing in Fig. 5, has -before the steady state- a frequency of 1.7 Hz and an amplitude of 45 *Nm*. The control signal appearing in Fig. 6, has -before the steady state- a frequency of 5.25 Hz and an amplitude of 32 *Nm*. The control signal appearing in Fig. 7, has - before the steady state- a frequency of 2.8 Hz and an amplitude of 48 *Nm*.
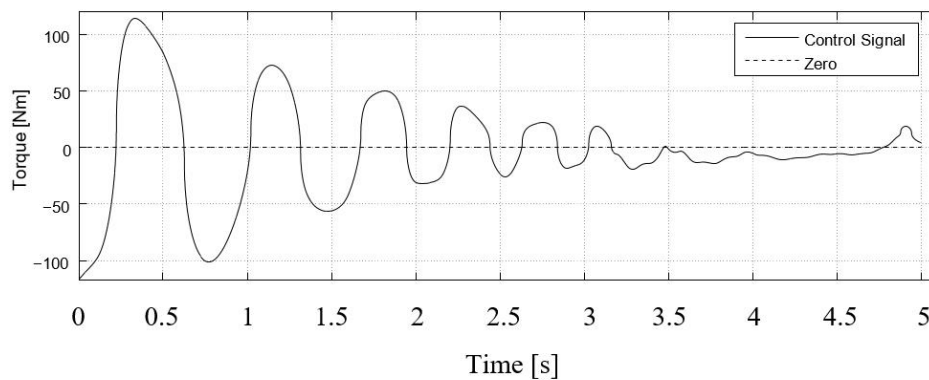
Fig. 5. Control signal to perform the behaviour of Fig. 2.
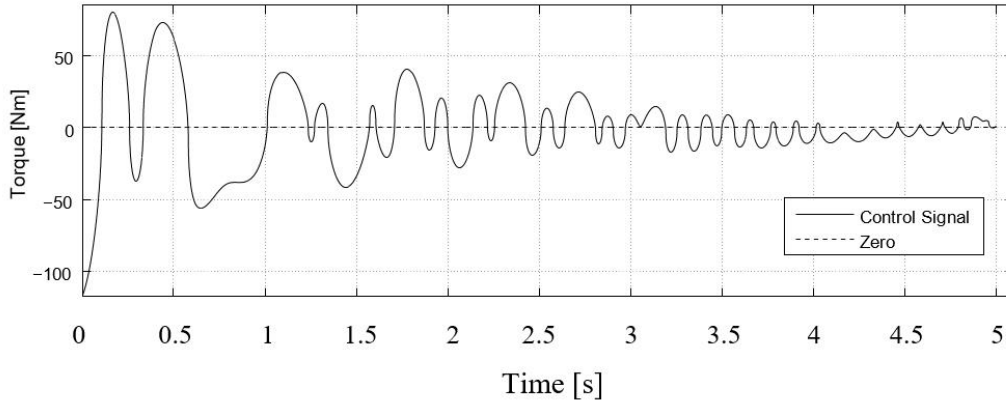
**Fig. 6.** Control signal to perform the behaviour of Fig. 3.
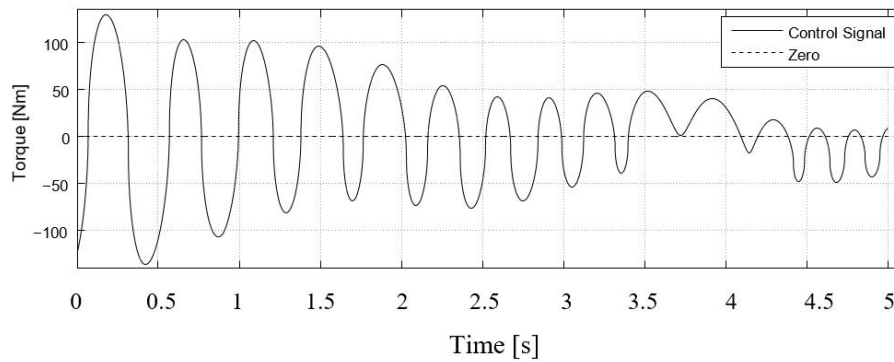
Fig. 7. Control signal to perform the behaviour of Fig. 4.

It is worth to mention that these values for both frequency and amplitude, are average values. The control signals in Figs. 5–7, are low in frequency and amplitude, the consequence of this fact is that the chattering-effect has been totally removed.

Figs. 8–10 are devoted to show the trajectory tracking for the first, second and third robot joints respectively, working with the lower limits of the α, β values located in the 3*rd* range. Fig. 8 shows the transient ending at 0.22 *s*, which represents 1/11.4 of the convergence time of Fig. 2. The actual chattering acting over this first joint in steady state has an average amplitude of 0.0217 *rad* with the same frequency of the control signal that produce it (*i.e.*, 1000 Hz).
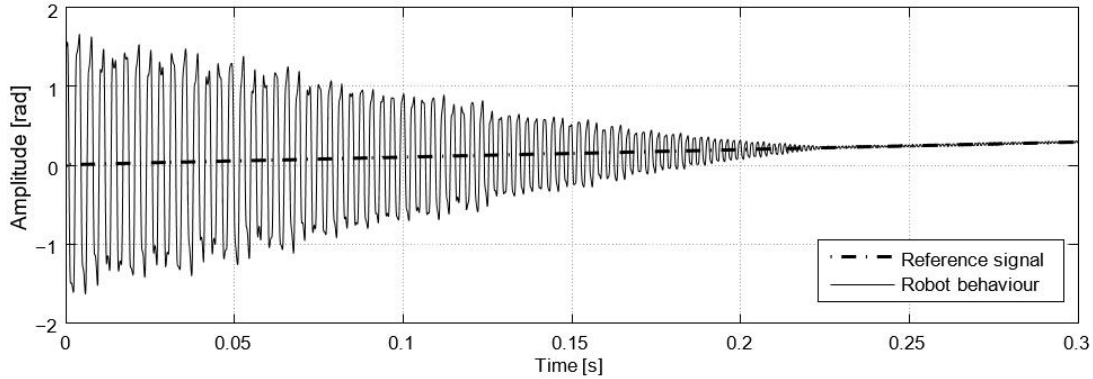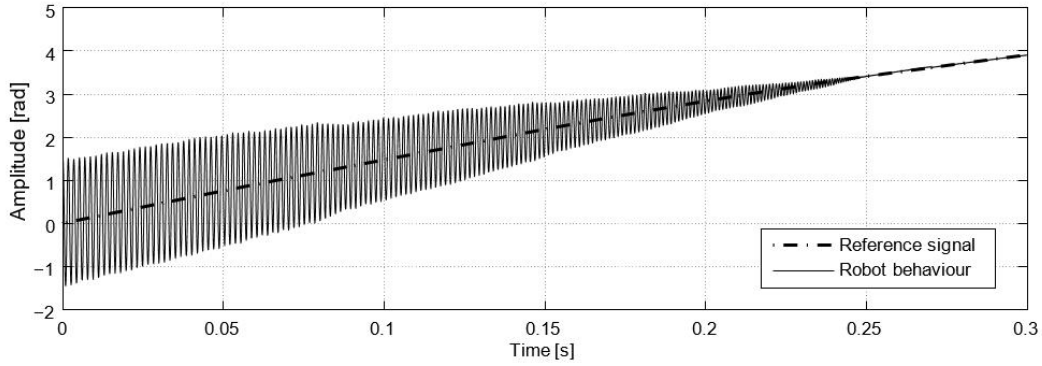
Fig. 8. Robot's first joint tracking the reference with $\alpha = 6.8 \times 10^6$ and $\beta = 55 \times 10^6$.

Fig. 9 shows the transient ending at 0.22 *s*, which represents 1/12.7 of the convergence time of Fig. 3. The actual chattering acting over the second joint in steady state has an average amplitude of 0.023 *rad* with the same frequency of the control signal that produce it (*i.e.*, 2900 Hz).
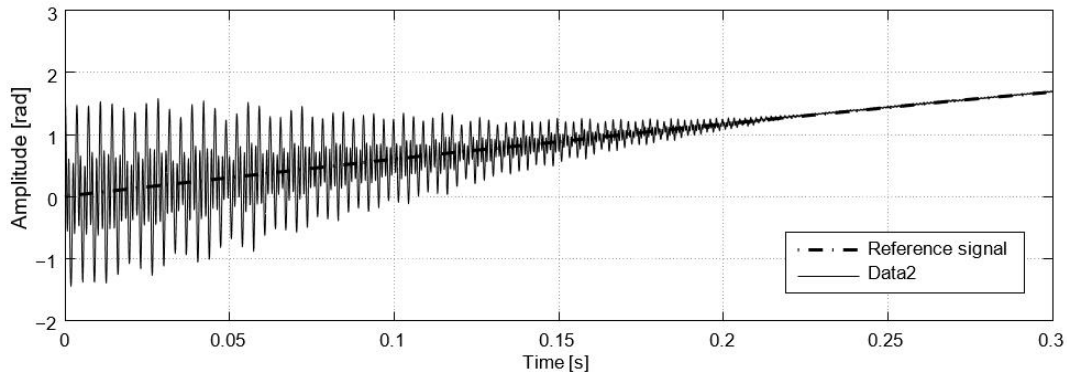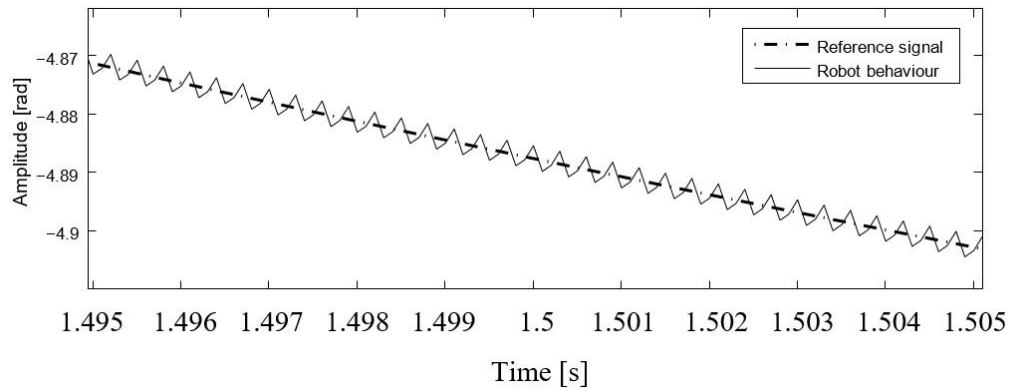

Fig. 9. Robot's second joint tracking the reference with $\alpha = 7.4 \times 10^6$ and $\beta = 57 \times 10^6$.

Fig. 10 shows the transient ending at 0.25 *s*, which represents 1/16.8 of the convergence time of Fig. 4. The actual chattering acting over the third joint in steady state has an average amplitude of 0.009 *rad* with the same frequency of the control signal that produce it (*i.e.*, 2500 Hz). *The increasing in the speed of convergence is a measure of the increased robustness of the controller.*

**Fig. 10.** Robot's third joint tracking the reference with $\alpha = 7.2 \times 10^6$ and $\beta = 60 \times 10^6$.

Fig. 11 is an enlarged view into the nearest of 1.5 s of the robot's third joint tracking the reference with $\alpha = 7.2 \times 10^6$ and $\beta = 60 \times 10^6$, to show the rejection of the disturbance caused by gravity (which appears en Fig. 4). Additionally, in this zoom it is possible to observe the characteristic shape of the chattering-effect, and the way in which the robot's joint remains attached to the reference signal.

Fig. 11. Zoom into the robot's third joint tracking the reference with $\alpha = 7.2 \times 10^6$ and $\beta = 60 \times 10^6$.

Figs. 12–14 are dedicated to show the control signal provided by the controller for the first, second and third robot joints respectively, working with the lower limits of the α, β values located in the 3rd range.

The control signal appearing in Fig. 12, has -for the steady state- a frequency of 1000 Hz and an amplitude of 7×10^5 Nm. For the transient stage has a frequency of 280 Hz and evidently it has a variable amplitude coming from 0.85×10^7 to 7×10^5 Nm.
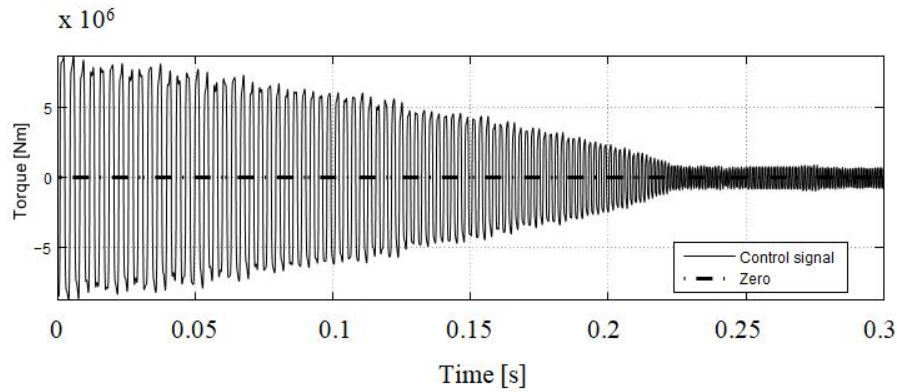
Fig. 12. Control signal to perform the behaviour of Fig. 8.

The control signal appearing in Fig. 13, has -for the steady state- a frequency of 2900 Hz and an amplitude of 8×10^5 Nm. For the transient stage has a frequency of 1000 Hz and evidently it has a variable amplitude coming from 0.9×10^7 to 8×10^5 Nm.
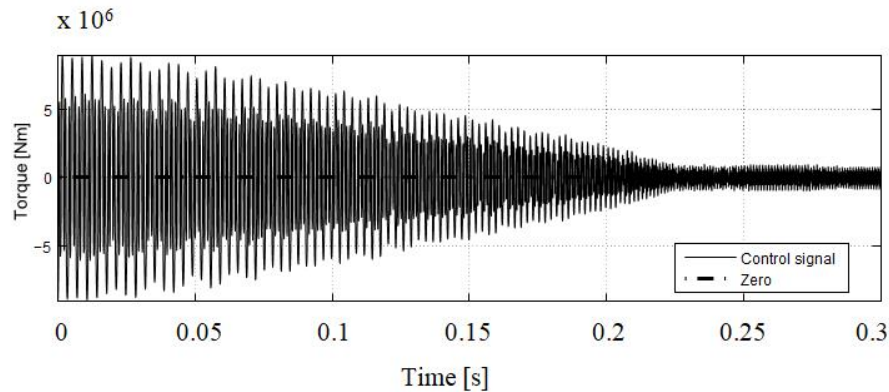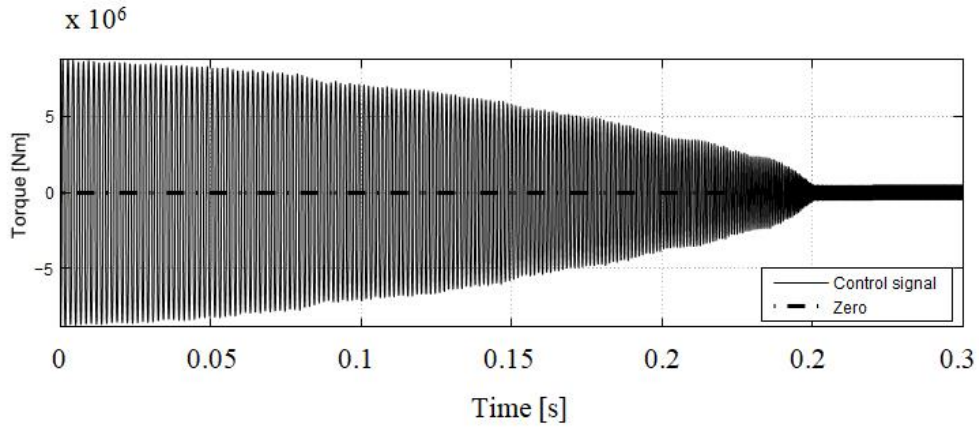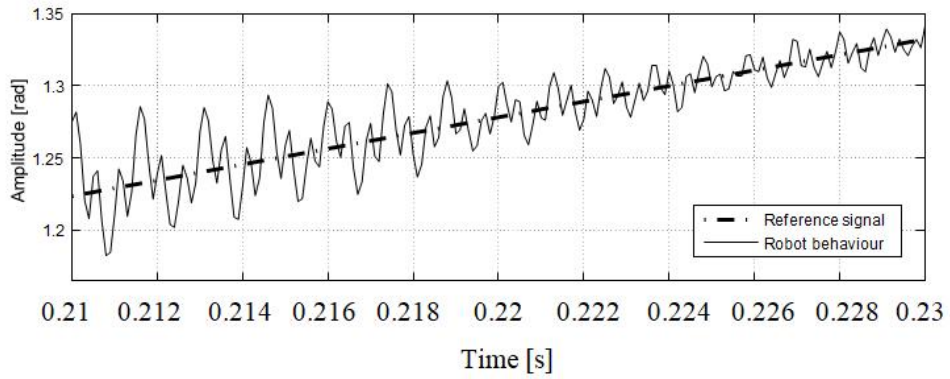

**Fig. 13**. Control signal to perform the behaviour of Fig. 9.

The control signal appearing in Fig. 14, has -for the steady state- a frequency of 2500 Hz and an amplitude of 4.85×10^5 Nm. For the transient stage has a frequency of 780 Hz and evidently it has a variable amplitude coming from 0.85×10^7 to 4.85×10^5 Nm.

Fig. 14. Control signal to perform the behaviour of Fig. 10.

Fig. 15. Zoom into the transitional stage from the transient to the steady state of Fig. 9.
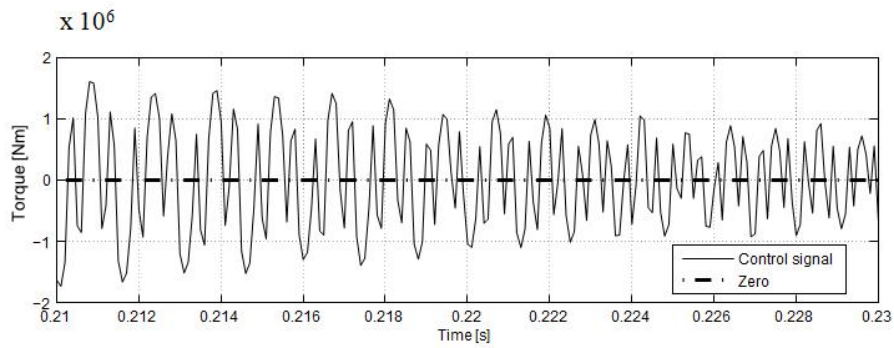
Fig. 16. Zoom into the transitional stage from the transient to the steady state of Fig. 13.

It is possible to observe a zoom inside a transitional stage from the transient to steady state for both the trajectory tracking in Fig. 15 and for the control signal behaviour in Fig. 16, referred to the second robot link and with high α-β values. These last two figures show that frequency and wave shape are the same for both position and torque, at any time.

Discussion

Results given by experiments performed with α and β located in the upper limit of the $1st$ range of values in Table 2, supports that, the STA working under the given conditions, causes a loss of system robustness when the chattering is reduced. Figs. 2–4 show that disturbances are not vigorously rejected.

Results given by Figs. 5–7, support that the STA has the capability to totally remove the chattering-effect, being that the control functions are smooth and low in both frequency and amplitude, and this produces a smooth tracking of the reference in steady state with a frequency value near to zero (*i.e.*, the robot does not vibrate in steady state), as it can be observed in Figs. 2–4. Results given by experiments performed with α and β located in the lower limit of the $3rd$ range of values in Table 2, supports that, the STA working under the given conditions, produces a rise in the level of chattering-effect when the system robustness is increased. Figs. 8–10 show a stronger and faster convergence than that obtained in Figs. 2–4, in addition Fig. 11 does not show disturbances caused by gravity in the nearest of 1.5 *s* as it is shown in Fig. 4.

As such, the following remarks are obtained:

- The chattering can be considered as an amount of energy injected to the control system.
- The control system needs energy to maintain robust properties.
- A significant reduction of energy, decreases the reaction power to reject disturbances.
- According to the first law of thermodynamics, it is impossible maintain robustness when the available energy decreases.

It is important to mention that in this work is not argumented that the STA fails under specific operational conditions, but it just lower the robust properties when it is tuned to produce lower chattering levels.

Simulation results obtained in this research support that for the STA:

$$\Psi \approx \Pi$$

(6)

Where:

$\Psi \in R^{n}$ represents the amount of chattering-effect, and $\Pi \in R^{n}$ represents the system robustness. Expression (6), can also takes the form:

$$\Psi = k\Pi$$

(7)

Where:

$k \in R$ is a non-negative constant, valued according with every specific application.

As a first approach to apply the proposed equation (7), herein is also proposed for practical purposes that the amount of chattering can be measured taken the angular velocity of its behavior, *i.e.*, the amplitude multiplied by the frequency of the tracking error. Further, the inverse of the convergence time is a practical measure of system robustness. Taken this criteria, and the data provided in the last section, the values for k for the values of α and β in the begin of third range of Table 2 can be obtained as:

$$k_1 = (0.0217rad)(1000hz)(1/0.22s) = 4.774rad$$

$$k_2 = (0.023rad)(2900hz)(1/0.22s) = 14.674rad$$

$$k_3 = (0.009rad)(2500hz)(1/0.25s) = 5.625rad$$

For the first, second and third robot's joints respectively. As it can be observed, equation (7) can be used in many ways, according to the criteria employed to define the amount of chattering, robustness, and the values for α and β. Can also be selected the average of k for a large range of α and β. A more extensive and deep study to characterize k is proposed for future works, along with a thermodynamic approach to measure Ψ.

Equation (7) is the main result of this work, and it is valid for the given working conditions and for the extended following conditions.

Including an explicit disturbance w in the plant under control, it yields to:

$$\dot{x} = f(x) + g(x)u + p(x)w$$
$$y = h(x)$$

(8)

Where:

x is still the vector for the system states, f is a bounded uncertainty, g represents the gain vector for the control for matched/unmatched uncertainties, and y is the system output vector.

The normal form proposed by Isidori, 1989, for (8) includes the transformation:

$$\dot{z}_1 = z_2$$
$$\dots$$
$$\dot{z}_r = b(\xi,\eta) + a(\xi,\eta)u$$
$$\dot{\eta} = q(\xi,\eta) + a(\xi,\eta)w$$
$$y = z_1$$

$$(9)$$

Where:

$\xi = [z_1 \dots z_r]^T$, and $\eta = [z_r + 1 \dots z_n]^T$. From (9) and with the previous knowledge that the systems relative degree $r = n = 2$, we can conclude that it is not possible to examine under what conditions there exist a static state feedback control $u(x)$ in which the output y is completely decoupled from the disturbance w as it is presented in (Isidori, 1989). Even more, this demonstrates that for this closed-loop control system do not exist Zero Dynamics. Nevertheless, for the control system, simulation results support that the *Disturbance Decoupling Problem* is solved by the control law (2) working under the specified conditions and with parameters of 3*rd*-Range in Table 2.

Using this reasoning we can infer that results given for the STA can be generalized for control systems including implicit/explicit, bounded/unbounded, and matched/unmatched uncertainties.

Even more, as it can be seen, there is a wide range of values for Φ, Γ_m, and Γ_M to satisfy conditions (3)–(4) with the α, β values of both the 1*st* and the 3*rd* ranges given by Table 2, ensuring finite time convergence for the STA.

In practice, certain ranges of values for α and β parameters of the STA, causes control instability, at least for a robotic plant as that given by (1) and under the specified working conditions. An open problem arising from this work is the mathematical formulation for the STA conditions (α, β values) under which a given control system becomes unstable (see 2*nd* range in Table 2).

There are implications of results obtained herein in actual practical applications. In most cases in which engineers design robust control systems, SMC is taken into account as a possible solution to deal with perturbed systems, and the aim of designers is to obtain robustness and rejection of chattering at the same time when HOSM are used to control electromechanical plants

(with relative degree equals two), as theory claims. This work will help engineers to narrow their expectations in this regard, posing the reality as it is in the practical implementation processes. A typical practical example in which engineers should put special attention, is in serial robotic plants, where each articulation of the robot is disturbed by the chattering-effect produced by neighboring joints, when system robustness is high. Remember that when the robot is operating on industrial environments, it has high robustness requirements.

Conclusions

The STA is a class of HOSM, which is capable to reduce the chattering-effect, however, results obtained in this work show that the drastically reduction of the chattering, reduces significantly the robustness for the control system.

Accordingly with expression (7) the chattering-effect produced by the HOSM can be considered as an amount of energy injected to the control system and a significant reduction of the chattering-effect via the HOSM may give rise to a control signal with low level of energy, and thus decreasing the reaction power in rejecting disturbances. This result is demonstrable at least for the outlined control conditions.

References

Alvarez Rodríguez, S., & Castañeda Hernández, C. E. (2015). A dual neural network as an identifier for a 3-DoF robot arm, International Journal of Advanced Robotic Systems, 12:40. DOI: 10.5772/58760.

Álvarez Rodríguez, S., Castañeda Hernández, C. E., Jurado, F., Morfín, O., & Esquivel, P. (2015). Real-time results for high order neural identification and block control

transformation form using high order sliding modes, Asian Journal of Control, Vol. 18, No. 3, pp. 1-17. Published online in Wiley Online Library (wileyonlinelibrary.com). DOI: 10.1002/asjc.1139.

Bartolini, G. (1989). Chattering phenomena in discontinuous control systems, Int. J. Systems Sci., vol. 20, pp. 2471-2481.

Bartolini, G., Ferrara, A., & Usani, E. (2002). Chattering avoidance by second-order sliding mode control, IEEE Transactions on Automatic Control, vol. 43-2, pp. 241-246.

Boiko, I., & Fridman, L. (2005). Analysis of chattering in continuous sliding mode controllers, IEEE Transactions on Automatic Control, 2012, vol. 50, no. 9, pp. 1442-1446.

Dorel, L., & Levant, A. (2008). On Chattering-Free, Proceedings of the 47th IEEE Conference on Decision and Control, Cancún, México.

Fridman, L. (2001). An averaging approach to chattering, IEEE Transactions on Automatic Control, vol. 46, pp.1260-1264.

Fridman, L., Moreno, J., & Iriarte, R. (2011). Sliding Modes after the First Decade of the 21st Century. State of the Art. Springer-Verlag, Berlin Heidelbert.

Furuta, K., & Pan, Y. (2000). Variable structure control with sliding sector, Automatica, vol. 36, pp. 211-228.

Furuta, K., & Pan, Y. (2003). Higher-order sliding modes, differentiation and output-feedback control, International Journal of Control, vol. 76-9, pp. 924-941.

Isidori, A. (1989). Nonlinear Control Systems Springer-Verlag, Berlin Heidelberg, New York. pp. 8, 137-185. 3-th edition.

Khalil, H. (2001). Nonlinear Systems, Prentice Hall, third edition.

Levant, A. (1993). Sliding order and sliding accuracy in sliding mode control, International Journal of Control, vol. 58, No. 6, pp 1247- 1263.

Levant, A. (2013). Advances in sliding mode control, Chapter 5: Practical Relative Degree Approach in Sliding-Mode Control, Springer-Verlag Berlin Heidelberg, pp 97-115.

Loukianov, A. G., Rivera, J., & Cañedo, J. M. (2002). Discrete-time sliding mode control of an induction motor, Proceedings of the 15th IFAC World Congress, Barcelona, Spain.

Morfín, O. (2009). Control por modos deslizantes integrales y de segundo orden del generador de inducción de rotor devanado en tiempo real, Instituto Politécnico Nacional, México, pp. 40.

Qu, Z., & Dawson, D. M. (1995). Robust tracking control of robot manipulators. IEEE press Piscataway, NJ, USA.

Sira-Ramírez, H. (2002). Dynamic Second-Order Sliding Mode Control of the Hovercraft Vessel, IEEE Transactions on Control Systems Technology, vol. 10, no. 6, pp. 860-865.

Spong, W. S., & Vidyasagar, M. (1989). Robot Dynamics and Control, John Wiley and Sons, New York, N.Y., USA.

Utkin, V., Guldner, J., & Shi, J. (1999). Sliding Mode Control in Electromechanical Systems, CRC Press, New York, N.Y., USA, pp. 1.